First publ. in: Journal of the Optical Society of America / B 27 (2010), 1, pp. 65-71

Numerical analysis of a sub-picosecond thin-disk laser oscillator with active multipass geometry showing a variation of pulse duration within one round trip

Joerg Neuhaus,[1,*] Dominik Bauer,[1,2] Jochen Kleinbauer,[2] Alexander Killi,[2] Dirk H. Sutter,[2] and Thomas Dekorsy[1]

[1]*Department of Physics and Center of Applied Photonics, University of Konstanz, 78457 Konstanz, Germany*
[2]*TRUMPF-Laser GmbH + Co. KG, Aichhalder Str. 39, 78713 Schramberg, Germany*
**Corresponding author: joerg.neuhaus@uni-konstanz.de*

The mode locking dynamics of a diode-pumped thin-disk laser oscillator with an active multipass cell operated in ambient atmosphere was studied numerically. The numerical results are compared to experimental results of a passively mode-locked thin-disk Yb:YAG laser with several megahertz repetition rate, sub-picosecond pulse duration, and >10 μJ pulse energy. The numerical simulations prove that the soliton area theorem predicts a correct pulse duration when considering an average pulse energy inside the oscillator. Furthermore, they show a variation in the full width at half-maximum pulse length for the pulse that propagates within the oscillator. This oscillation shows a behavior that is contrary to a change in the pulse length given by the soliton area theorem when considering the real pulse energies at respective points in the resonator. The "breathing" is caused by the strong influence of the self-phase modulation of the ambient atmosphere and large amounts of dispersion resulting in a deviation from the sech^2 pulse shape and a chirped pulse.

OCIS codes: 140.3430, 140.4050, 140.3480, 140.3580.

1. INTRODUCTION

Ultrashort laser pulses in the microjoule regime are of prime importance for a variety of applications, including high-speed micro-machining [1], pumping of optical parametric oscillators, as well as basic research, e.g., in high-field physics or for the generation of intense terahertz pulses [2–6]. As compared to oscillator-amplifier configurations [3,7], ultrafast oscillators are very attractive due to their simplicity and compactness. To some extent microjoule pulse energies from an oscillator can be obtained by using extended resonator cavities [5,6,8,9] or by cavity dumping [10,11]. In order to reach high average powers together with high pulse energies, a thin-disk (TD) laser crystal is the medium of choice [12], allowing for true power scalability by increasing the beam size and exploiting the excellent cooling properties of the disk. However, the relatively low gain of a TD laser and the resulting high intra-cavity powers have to be overcome.

Previous pulse energies obtained directly from an oscillator in ambient atmosphere were limited to energies below 2 μJ caused by the strong self-phase modulation (SPM) of air [13]. Higher pulse energies were obtained in a He-flooded cavity with pulse energies of 11 μJ [5] at sub-picosecond pulse lengths. Another way to decrease the SPM is to use larger output-coupling (OC) rates in combination with a high-gain medium.

Recently, we have reported on a laser oscillator with multiple passes through the gain medium by the use of an active multipass cell (AMC). The cavity setup is shown schematically in Fig. 1 [14]. External pulse energies of up to 25.9 μJ [15] have been achieved with OC rates of up to 78%. In general, the mode locking mechanism of laser oscillators is very well understood numerically and for some laser geometries also analytical solutions can be found [16]. However, to our knowledge, no analysis of a solitary mode-locked laser oscillator with large OC rates and highly dispersive and nonlinear elements has been performed so far. Numerical analyses of cavity-dumped systems [17] or mode-locked fiber lasers [18] are similar to the analysis of a laser with an AMC; however, no detailed analysis has been performed for comparable parameters so far. Because of the large OC rates the approximations made in the Haus master equation of mode locking are not applicable. Hence, we have performed a detailed numerical analysis of the mode locking behavior of a laser geometry similar to that reported in [15]. Here, detailed results from numerical simulations of the evolution of the electric field within the resonator are being reported.

This paper is organized as follows: After a brief description of the laser setup and the details of the numerical simulation in Section 2, the parameters for simulating the experimental results presented in [15] are discussed (Section 3). In Section 4, a modified soliton area theorem for large OC rates [15] is proposed and proved by the simulation. In Section 5, the pulse dynamics of a laser with an AMC is described, showing an oscillation in FWHM pulse duration within every round trip.

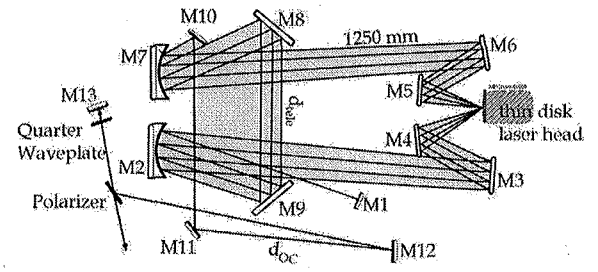

Fig. 1. Schematic design of an AMC cavity, as it was simulated here and was used in the experiments demonstrated in [15]. Most of the mirrors were highly dispersive mirrors. For starting and stabilizing the mode locking, mirror M13 was replaced with a SESAM. Whereas here only four passes through the AMC are shown, up to 13 passes have been realized.

2. NUMERICAL SIMULATIONS

Because of the large OC rate, the linearized Haus master equation of mode locking [16,19] is not applicable for simulating a laser with an AMC. Instead, mode locking was simulated numerically by the repetitive action of the various optical components on the electric field v in the time or frequency domain as suited best for the respective component. This approach is shown schematically in Fig. 2 and can be written symbolically in the time domain as

$$v(t+T_R)=\prod \hat{O}_i v(t). \tag{1}$$

Here $\hat{O}_i$ is the operator for the ith optical element. The operators for gain, loss, group delay dispersion (GDD), and SPM are given by

$$\hat{O}_{\text{gain}}(t)=g(\omega,t)N^*\frac{\partial^2}{\partial t^2},$$

$$\hat{O}_{\text{loss}}(t)=\sqrt{1-l(t)},$$

$$\hat{O}_{\text{GDD}}(t)=iD_2\frac{\partial^2}{\partial t^2},$$

$$\hat{O}_{\text{SPM}}(t)=\exp(-i\gamma_{\text{SPM}}|v|^2),$$

where $l(t)$ is the power loss; $g(\omega,t)$ is the power gain with

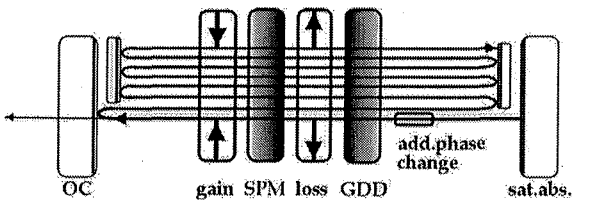

Fig. 2. Schematic of the numerical simulation, demonstrating the repetitive action of the various operators within the AMC as given by Eq. (1). Any additional SPM or GDD is included in the symbol labeled "add. phase change."

$$g(\omega,t)=\frac{g(T)}{1+\left(\dfrac{\omega-\omega_g}{\Delta\omega_g}\right)^2}, \tag{2}$$

where T represents times large compared to the pulse duration; N^* is the number of passes through the gain medium (in this case it is 2 for every action of the operator); γ_{SPM} is the SPM coefficient; D_2 is the amount of dispersion; ω_g is the center gain frequency; and $\Delta\omega_g$ is the gain bandwidth given by $(\Delta\omega_L/2\cdot)\sqrt{g_0/g(T)}$, where $\Delta\omega_L$ is the inherent amplification bandwidth of the gain medium and g_0 is the small signal gain. The operators $\hat{O}_i$ have been applied on the electric field v in the time or frequency domain analogous to the split-step Fourier method [20] implemented within a Matlab environment.

Furthermore, the gain $g(T)$ and saturable loss $l(t)$ were numerically calculated according to the common rate equations,

$$\frac{\partial g(T)}{\partial T}=-\frac{g(T)-g_0}{\tau_{\text{eff}}}-\frac{|v|^2}{E_{\text{sat,g}}}g(T), \tag{3}$$

$$\frac{\partial l(t)}{\partial t}=-\frac{l(t)-l_0}{\tau_l}-\frac{|v(t)|^2}{E_{\text{sat,l}}}l(t), \tag{4}$$

where τ_{eff} corresponds to the effective relaxation time of the gain medium; g_0 to the small signal gain; l_0 to the saturable losses; $E_{\text{sat,g/l}}$ to the saturation energies of the gain and loss media, respectively; and τ_l to the relaxation time of the saturable absorber. Acting on the electric field in the frequency domain, the gain $g(T)$ was taken as constant for one pass of the pulse over the gain medium, a reasonable approximation for a TD solid-state gain medium.

Additionally, the small signal gain and the saturation energy of the gain medium were calculated numerically by using a rate equation for the gain and laser intensity with an inversion parameter,

$$\beta(I^{(P)},I^{(L)})=\frac{\dfrac{I^{(L)}}{h\nu^{(L)}}\sigma_{abs}^{(L)}+\dfrac{I^{(P)}}{h\nu^{(P)}}\sigma_{abs}^{(P)}}{\dfrac{I^{(L)}}{h\nu^{(L)}}\{\sigma_{abs}^{(L)}+\sigma_{em}^{(L)}\}+\dfrac{I^{(P)}}{h\nu^{(P)}}\{\sigma_{abs}^{(P)}+\sigma_{em}^{(P)}\}+1/\tau_f}, \tag{5}$$

averaged over the disk with a Gaussian intensity distribution of the laser mode and with a super-Gaussian intensity distribution of the pump mode. Here, the various σ's are the corresponding emission (em) and absorption (abs) cross sections for pump (P) and laser light (L), τ_f is the fluorescence lifetime of the laser medium, and $h\nu$'s are the photon energies for pump (P) and laser light (L). The pump distribution of the experimentally realized laser was measured with a camera based system, showing good agreement with a super-Gaussian intensity distribution of eighth order. The intensity of the pump and laser mode, given by summing over all intensities of the respective beams incident on the gain medium within one round trip,

$$I^{(L/P)} = \sum_{i}^{N^{(L/P)}} I_i^{(L/P)}, \quad (6)$$

was taken as constant in the direction of propagation through the TD and the spectroscopic data of ytterbium-doped yttrium aluminum garnet (Yb:YAG) was used. The small signal gain and saturation intensity were first determined according to the measured output power for continuous wave (CW) laser operation, which were assumed to be the same for the mode-locked case. Very good agreement between the simulation and an experimental Rigrod type analysis [21], i.e., efficiency over the OC rate, for four passes through the AMC was found. Performing a real Rigrod analysis [21] showed a slightly different efficiency curve because this kind of analysis does not include any saturation effects of the pump absorption. However, when setting the pump light absorption in the simulation constant the simulation was perfectly proved by a Rigrod analysis [21], showing not only the same efficiency curve, but also resembling exactly all obtainable parameters.

In Fig. 3 the efficiency over the OC rate is shown for a TD laser comprising an AMC with 4–60 passes per round trip (four passes through the TD correspond to one pass through the AMC). OC rates of >70% at high efficiencies are easily available for a large number of passes through the TD. In the simulation a constant loss of 0.6% per pass through the AMC, a TD similar to that used in the experiments, a Gaussian laser mode width of 0.95 mm, and a super-Gaussian ($n=8$) pump mode width of 1.05 mm were used. The pump power was absorbed at absorption rates of 70%–80% within 20 passes through the TD.

3. SIMULATING THE EXPERIMENTS

Simulations have been performed to predict the mode locking of the laser with 11 passes through the AMC as presented in [15]. The parameters used to simulate the mode locking of the laser according to Eq. (1) and the resulting data are listed in Table 1. Pump powers in between 80 W to 165 W with a step size of 5 W were simulated. Only the results for the lowest and highest pump powers are shown in Table 1. As presented in Fig. 2 of [14], good agreement between experimental and simulated data was found. As fit parameters, the actual GDD and the third order dispersion were adjusted for best agreement (see Fig. 5 in [15]).

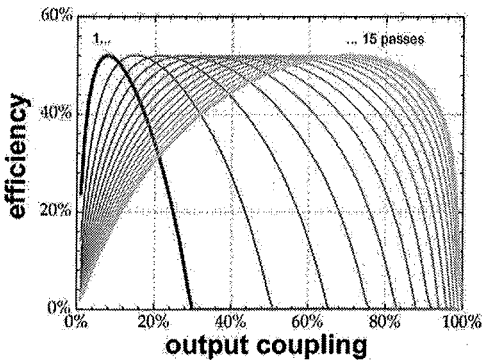

Fig. 3. (Color online) Simulated laser efficiency for a TD laser, comprising an AMC while operating in CW mode. The figure shows the laser behavior for 1–15 passes through the AMC, thereby shifting the peak efficiency further to the right.

Table 1. Parameters Used for the Numerical Simulations of the Experiments (Upper Part) and Respective Results (Lower Part)

Cavity length (m)	44.15
OC rate	64%
Passes through AMC	11
TD/spot-size laser/pump mode (μm)	TD_{60}/980/1100
SESAM/spot size (μm)	$SESAM_{B1}$/400,...,500
Modulation depth of SESAM	0.8%
Relaxation time of SESAM (ps)	1
Saturation fluence of SESAM	34 μJ/cm^2
HDCM within/outside of AMC	6/5
Pump power (W)	80,...,165
Gain bandwidth $\Delta\lambda$ (nm)	6.5 nm
Number of round trips	<10,000
Total GDD per round trip (ps^2)	−0.1787
SPM per round trip (10^{-3}/MW)	37.477
B-integral	0.0684,...,0.556
External pulse energy (μJ)	6,...,17.2
Pulse length τ_P (fs)	2840,...,1010
$\Delta\lambda$ (nm)	0.4,...,1.12
Small signal gain per pass through TD	0.0816,...,0.1131
Pump power absorbed	74.1%,...,72.5%
TBP	0.3166,...,0.3211
Soliton order (see [17])	1.255,...,1.277
Total mirror loss per round trip	21.65%

As a starting fit parameter for all simulations, the mirror loss was adjusted until an agreement between simulated and experimental output powers was given for the applied pump power. For all further simulations with less pump power the loss was taken as constant. A resulting loss of 22%, corresponding to a loss of ≈0.15% per mirror bounce, is in accordance with a reflectivity of ≈99.85% for the highly dispersive chirped mirrors (HDCMs) providing most reflections and considering further loss caused by the $\lambda/4$-wave plate or semiconductor saturable absorber mirror (SESAM).

Simulations of the pulse shaping in the laser cavity starting with an arbitrary sech^2 pulse resulted in stable mode locking for pump powers in between 80 and 165 W and parameters as in Table 1. Similar to the experimental results, for pump powers below 80 W Q-switching was observed in the simulation and for pump powers larger than 165 W double pulses occurred.

4. DECREASING THE OC RATE

In order to investigate the influence of the OC rate on the pulse dynamics, simulations with constant internal energy, i.e., before the output coupler, and decreasing OC rate have been performed. Without coupling out the soliton exhibits parameters that agree with the soliton area theorem [22],

$$\tau_P \approx \frac{1.76 \cdot 2|\beta_2|}{\gamma_{\mathrm{SPM}} E_{P,\mathrm{int}}}, \tag{7}$$

with β_2 representing the amount of the GDD, γ_{SPM} the SPM coefficient, and $E_{P,\mathrm{int}}$ the internal pulse energy. For large OC rates, however, the soliton area theorem is not the right choice for approximating the pulse length of the generated pulses, because the pulse energy inside the resonator is not constant within one round trip. A modification of the soliton area theorem, using an average pulse energy inside the cavity by assuming an exponential increase in the pulse energy with an external pulse energy of $E_{P,\mathrm{ext}}$, is given by [15]

$$\tau_P \approx \frac{-1.76 \cdot 2|\beta_2| \ln(1 - \mathrm{OC})}{\gamma_{\mathrm{SPM}} E_{P,\mathrm{ext}}}. \tag{8}$$

The resulting pulse duration for various amounts of OC rates is shown in Fig. 4(a), together with the results from the numerical simulations. The parameters that were different compared to those in Table 1 are listed in Table 2. Simulations were performed at OC rates between 0% and 64%, while keeping the internal pulse energy constant. Only results for the lowest and highest OC rates are listed. The total mirror loss per round trip was decreased in this simulation to only 2% in order to simulate a nearly unperturbed soliton for zero OC rate. In Fig. 4(b) the spectrum for the various OC rates is shown. Due to the temporally shorter pulses, the spectral width increases with decreasing OC rate. For zero OC, stable soliton propagation was observed with a constant pulse duration of the soliton while propagating through the laser cavity. While for large OC rates Kelly sidebands are visible in the spectrum, they disappear for zero OC.

Table 2. Parameters Used for the Numerical Simulations of Various OC Rates (Upper Part) with Respective Results (Lower Part)

Pump power (W)	135,...,20
OC rate	64%,...,0%
HDCM within/outside of AMC	6/0
Total GDD per round trip (ps^2)	−0.172
B-integral	0.5,...,0.926
Internal pulse energy (μJ)	25.3
Pulse length τ_{FWHM} (fs)	1196,...,765
$\Delta\lambda$ (nm)	1.06,...,1.47
Small signal gain per pass through TD	0.106,...,0.0292
Pump power absorbed	73%,...,75.5%
TBP	0.32,...,0.316
Soliton order	1.27,...,1.003
Deviation from soliton shape	−0.2%,...,0%
Total mirror loss per round trip	2%

5. PULSE DYNAMICS WITHIN ONE ROUND TRIP

For large OC rates and operation in ambient atmosphere the FWHM pulse length of the soliton was found to oscillate within each round trip as shown in Fig. 5. This effect was found to be especially strong for sub-picosecond pulses. According to the soliton area theorem an increase in the pulse length is expected after the output coupler because of the decrease in the pulse energy. Such a behavior was observed when simulating an unperturbed propagation of this soliton after the output coupler without any gain and loss, but otherwise similar parameters as they exist within the laser. However, in the simulation of this laser a decrease in the pulse length was observed instead. In Fig. 5(a) the FWHM pulse length oscillation is compared to the calculated pulse length according to the soliton area theorem considering the pulse energy, the GDD, and the SPM within every section of the oscillator. The specific parameters used in the simulations are listed in Table 3. Because of the stronger effect for shorter pulses and the availability of materials with larger bandwidths [23], a gain material with about three times larger bandwidth was used in the simulation, resulting in a FWHM pulse length of 600 fs. As we used at maximum 13 passes through the AMC with an OC rate of 80% in previous experiments [15], the simulation was carried out accordingly.

Five specific points at positions of 13.1, 22.9, 32.7, 55.6, and 88.3 m have been highlighted. These positions were chosen because of being unique either geometrically or because of their corresponding pulse parameters. The first is located right behind the output coupler, the second has the shortest pulse duration, the third is showing a turn-

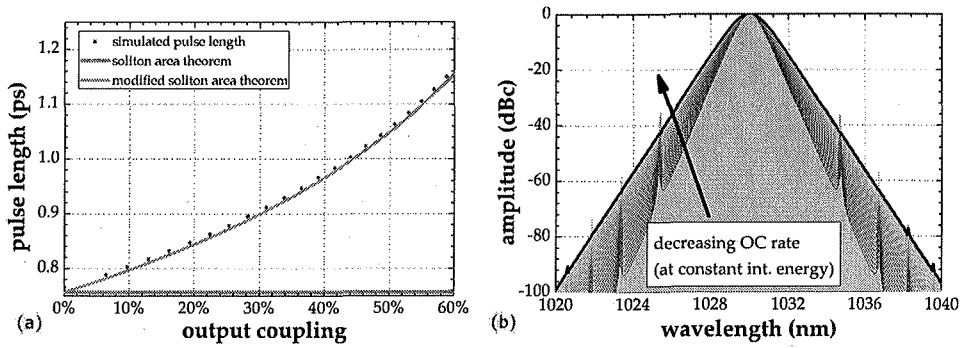

Fig. 4. (Color online) (a) Pulse duration over OC rate as given by numerical simulations for 11 passes through the AMC, showing the applicability of the soliton area theorem at an OC rate of 0%. For large OC rates, however, the modified version of the soliton area theorem as given by Eq. (8) must be used. (b) Spectra for various OC rates starting at 64% and ending at 0% OC rate. For non-vanishing OC rates Kelly sidebands appear.

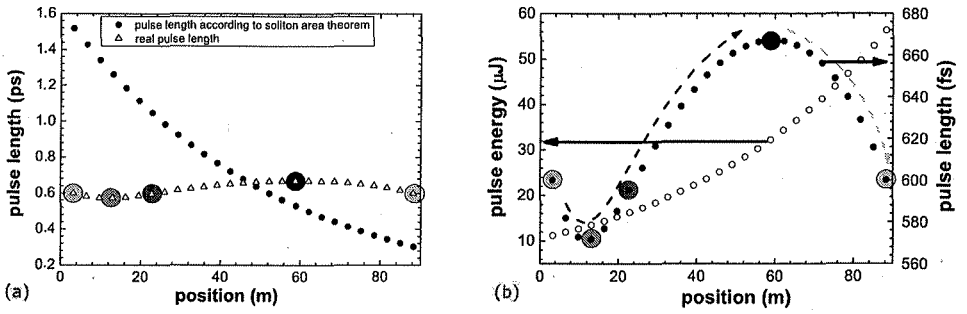

Fig. 5. (Color online) (a) FWHM pulse length as determined by the numerical simulation and the soliton area theorem. Every symbol (dot or triangle) corresponds to the soliton just before passage over the TD or through the output coupler. (b) FWHM pulse length as determined by the numerical simulation on a larger scale, together with a pulse energy increase inside the resonator. Dashed arrows mark a change in chirp, whereas larger colored circles refer to positions during a round trip which are discussed in the text and the following figures.

ing point in the FWHM pulse duration, the fourth has the largest amount of pulse duration, and the last position is right before the output coupler. In the following, the properties of the pulse at these positions in particular will be discussed or highlighted in the remaining figures for a detailed understanding of the pulse dynamics within the oscillator.

In Fig. 5(b) the change in the FWHM pulse duration for one complete round trip is plotted together with the actual pulse energies within the resonator. The change in the FWHM pulse duration is caused by two reasons. First of all the pulse experiences a chirp and second the shape of the pulse deviates from that of an ideal sech^2 pulse. The chirp is simply caused by a mismatch of the SPM and GDD at different positions within the resonator. The local B-integral per section, being a measure for the SPM, is shown in Fig. 6(a) together with the local GDD per unit length. The GDD is constant for the total length of the resonator because of the choice of self-similar GDD-mirrors. For a linear cavity as considered here, it is generally not possible to introduce a different amount of dispersion acting on the pulse on its way from the output coupler to the opposite end mirror, compared to the dispersion on its way back to the output coupler. However, due to the exponential increase in the pulse energy, this is the case for the amount of the SPM.

Table 3. Parameters Used for the Numerical Simulations of a Larger Gain Bandwidth (Upper Part) with Respective Results (Lower Part)

Cavity length (m)	44.15
OC rate	80%
Passes through AMC	13
HDCM within AMC	6
Pump power (W)	350
Gain bandwidth $\Delta\lambda$ (nm)	$3\times(6.5$ nm)
Number of round trips	5000
Total GDD per round trip (ps^2)	−0.189
SPM per round trip (10^{-3}/MW)	38.89
B-integral	1.47
External pulse energy (μJ)	45
Pulse length τ_P (fs)	600
$\Delta\lambda$ (nm)	1.79
Small signal gain per pass through TD	0.1383
Pump power absorbed	72.26%
TBP	0.3033
Soliton order (see [17])	1.3828
Total mirror loss per round trip	11.33%

In Fig. 6(b) the group delay is plotted for all five points mentioned before. A strong positive chirp is visible for the pulse situated around the output coupler at 0 and 88.3 m. On the contrary the chirp at a position of 55.6 m is negative and even vanishes at about 22.9 m. This behavior can be easily explained by the predominance of the GDD within the first part and the predominance of the SPM within the last part of one round trip as shown in Fig. 6(a).

Even though the chirp varies at positions of 0 and 22.9 m, the FWHM pulse duration at these positions is similar. Since the spectral width remains constant for all positions within one complete round trip, this can only be explained by a varying pulse shape. In Fig. 7(a) the residual of the temporal pulse trace when compared with an ideal sech^2 is shown. The residuals at all five specific points have been plotted in detail in Fig. 7(b). Here one can see a deviation of the pulse shape at 0 m from an ideal sech^2, having an elevated peak, but stronger wings at both sides, which is opposite to the pulse shape deviation at 22.9 m, showing a "more Gaussian-shaped" peak. The pulse length evolution for a similar cavity setup but pulses with less external energy and picosecond pulses is qualitatively the same; only the variation in the pulse length is much smaller (only up to 0.4% change for pulses with 1200 fs duration and 16 μJ energy).

The deviation from the real pulse length compared to that according to the soliton area theorem as shown in Fig. 5(a) is therefore caused by the interplay of gain, GDD, and SPM within the laser. When "switching off" all gain and loss elements in the simulation right after the output coupler, the soliton ultimately increases its width slowly within multiple round trips until agreement with the pulse duration as given by the soliton area theorem is established. Since the spectral bandwidth remains constant for the pulse while propagating through the cavity, the time–bandwidth product (TBP) evolves similar to the pulse duration during one round trip.

Experiments have been performed proving this oscillat-

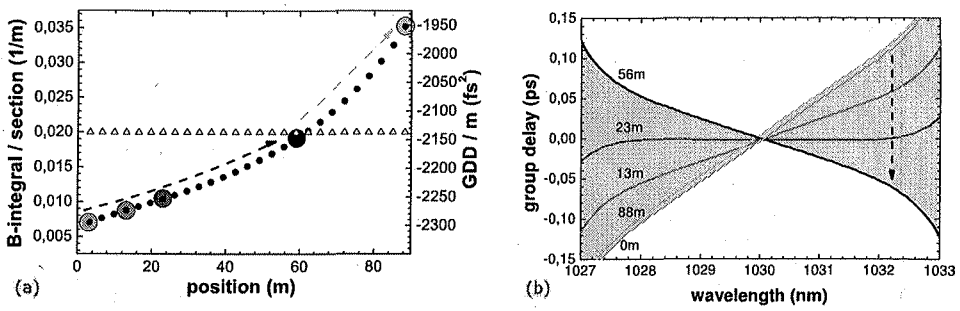

Fig. 6. (Color online) (a) B-integral and GDD for each section in between two passes through the gain medium of the AMC laser. The large colored circles are highlighting five specific points that are mentioned in detail in the text. (b) Group delay of the pulse at all five marked positions shown in corresponding colors.

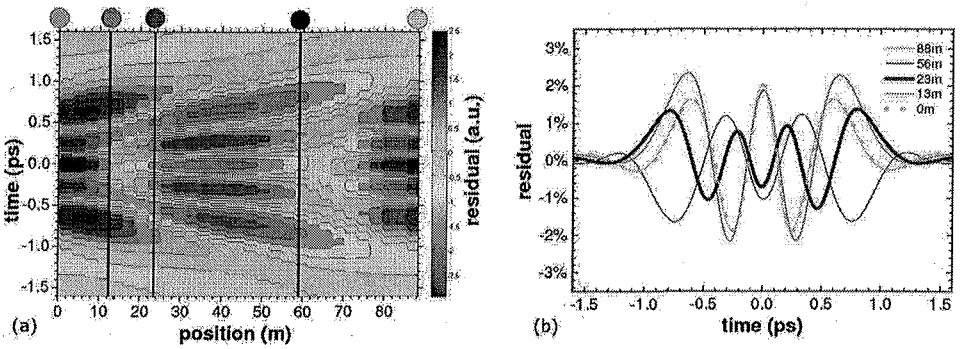

Fig. 7. (Color online) Residual of the temporal shape of the pulse while propagating within the oscillator compared to an ideal sech^2 pulse shape. The residuals at all five previously mentioned points are also shown in the diagram on the right side (b) with the specified positions resembling the correspondingly marked positions in (a). At some positions within the resonator, the pulse shows stronger wings and a more distinct peak compared to an ideal sech^2 shape.

ing behavior of the pulses inside the cavity. However, experiments were only performed for picosecond pulses with rather small changes in the pulse duration.

Simulations have been performed for different relaxation times (starting from some hundred femtoseconds to 10 ps) of the SESAM; no major differences in the pulse shaping dynamics were observed. However, the modulation depth of the SESAM had strong influence on the achievable pulse lengths, which were limited by the observance of instabilities, e.g., double pulses.

6. RESULT AND CONCLUSION

We presented detailed numerical results on an unamplified solid-state laser oscillator comprising an active multipass cavity while being operated in an ambient atmosphere. The numerical simulations of the electric field evolution within the cavity showed (i) very good agreement with experimental results, (ii) stable soliton propagation for zero output-coupling (OC) rate, (iii) agreement with a modified soliton area theorem for large OC rates, and (iv) oscillation in FWHM pulse duration within each round trip for large OC rates.

Knowledge of this oscillating pulse dynamics is important for understanding possible deviations from an ideal sech^2 pulse shape and a chirped pulse output. This is also essential for optimizing a laser oscillator with an active multipass cell (AMC) for the generation of sub-picosecond pulses at large pulse energies. The pulse length dynamics that has been described here might be even stronger for additional cavity elements such as a Herriott cell, for example, due to a stronger asymmetry in the SPM compared to that mentioned here.

ACKNOWLEDGMENTS

This work was partly funded by the German Federal Ministry of Education and Research, (contract 13N8580) and by a grant from the Ministry of Science, Research, and the Arts of Baden-Württemberg.

REFERENCES

1. B. N. Chichkov, C. Momma, S. Nolte, F. von Alvensleben, and A. Tünnermann, "Femtosecond, picosecond and nanosecond laser ablation of solids," Appl. Phys. A **63**, 109–115 (1996).
2. F. Brunner, E. Innerhofer, S. V. Marchese, T. Südmeyer, R. Paschotta, T. Usami, H. Ito, S. Kurimura, K. Kitamura, G. Arisholm, and U. Keller, "Powerful red-green-blue laser source pumped with a mode-locked thin disk laser," Opt. Lett. **29**, 1921–1923 (2004).
3. L. Shah, M. E. Fermann, J. W. Dawson, and C. P. J. Barty, "Micromachining with a 50 W, 50 μJ, subpicosecond fiber laser system," Opt. Express **14**, 12546–12551 (2006).
4. M. C. Hoffmann, K.-L. Yeh, H. Hwang, T. Sosnowski, B. S. Prall, J. Hebling, and K. A. Nelson, "Fiber laser pumped high average power single-cycle terahertz pulse source," Appl. Phys. Lett. **93**, 141107 (2008).
5. S. V. Marchese, C. R. Baer, A. G. Engqvist, S. Hashimoto, D. J. Maas, M. Golling, T. Südmeyer, and U. Keller, "Femtosecond thin-disk laser oscillator with pulse energy beyond the 10-microjoule level," Opt. Express **16**, 6397–6407 (2008).

6. T. Südmeyer, S. V. Marchese, S. Hashimoto, C. R. E. Baer, G. Gingras, B. Witzel, and U. Keller, "Femtosecond laser oscillators for high-field science," Nat. Photonics **2**, 599–604 (2008).
7. F. Röser, D. Schimpf, B. Ortac, K. Rademaker, J. Limpert, and A. Tünnermann, "90 W average power 100 μJ energy femtosecond fiber chirped-pulse amplification system," Opt. Lett. **32**, 2230–2232 (2007).
8. S. Naumov, A. Fernandez, R. Graf, P. Dombi, F. Krausz, and A. Apolonski, "Approaching the microjoule frontier with femtosecond laser oscillators," New J. Phys. **7**, 216–227 (2005).
9. S. Dewald, T. Lang, C. D. Schröter, R. Moshammer, J. Ullrich, M. Siegel, and U. Morgner, "Ionization of noble gases with pulses directly from a laser oscillator," Opt. Lett. **31**, 2072–2074 (2006).
10. A. Killi, A. Steinmann, J. Dörring, U. Morgner, M. J. Lederer, D. Kopf, and C. Fallnich, "High-peak-power pulses from a cavity-dumped Yb:$KY(WO_4)_2$ oscillator," Opt. Lett. **30**, 1891–1893 (2005).
11. G. Palmer, M. Emons, M. Siegel, A. Steinmann, M. Schultze, M. J. Lederer, and U. Morgner, "Passively mode-locked and cavity-dumped Yb:$KY(WO_4)_2$ oscillator with positive dispersion," Opt. Express **15**, 16017–16021 (2007).
12. A. Giesen, H. Hügel, A. Voss, K. Wittig, U. Brauch, and H. Opower, "Scalable concept for diode-pumped high-power solid-state lasers," Appl. Phys. B **58**, 365–372 (1994).
13. E. Innerhofer, T. Südmeyer, F. Brunner, R. Häring, A. Aschwanden, R. Paschotta, C. Hönninger, M. Kumkar, and U. Keller, "60 W average power in 810 fs pulses from a thin-disk Yb:YAG laser," Opt. Lett. **28**, 367–369 (2003).
14. J. Neuhaus, J. Kleinbauer, A. Killi, S. Weiler, D. H. Sutter, and T. Dekorsy, "Passively mode-locked Yb:YAG thin-disk laser with pulse energies exceeding 13 μJ by use of an active multipass geometry," Opt. Lett. **33**, 726–729 (2008).
15. J. Neuhaus, D. Bauer, J. Zhang, A. Killi, J. Kleinbauer, M. Kumkar, S. Weiler, M. Guina, D. H. Sutter, and T. Dekorsy, "Subpicosecond thin-disk laser oscillator with pulse energies of up to 25.9 microjoules by use of an active multipass geometry," Opt. Express **16**, 20530–20539 (2008).
16. H. A. Haus, "Mode locking of lasers," IEEE J. Sel. Top. Quantum Electron. **6**, 1173–1185 (2000).
17. A. Killi and U. Morgner, "Solitary pulse shaping dynamics in cavity-dumped laser oscillators," Opt. Express **12**, 3397–3407 (2004).
18. M. A. Abdelalim, Y. Logvin, D. A. Khalil, and H. Anis, "Properties and stability limits of an optimized mode-locked Yb-doped femtosecond fiber laser," Opt. Express **17**, 2264–2279 (2009).
19. H. A. Haus, "Theory of mode locking with a slow saturable absorber," IEEE J. Quantum Electron. **11**, 736–746 (1975).
20. G. Agrawal, *Nonlinear Fiber Optics* (Academic, 2001), Vol. 3.
21. W. W. Rigrod, "Saturation effects in high-gain lasers," J. Appl. Phys. **36**, 2487–2490 (1965).
22. F. X. Kärtner, I. D. Jung, and U. Keller, "Soliton mode-locking with saturable absorbers," IEEE J. Sel. Top. Quantum Electron. **2**, 540–556 (1996).
23. F. Brunner, T. Südmeyer, E. Innerhofer, F. Mourier-Genoud, R. Paschotta, V. E. Kisel, V. G. Shcherbitsky, J. Gao, K. Contag, A. Giesen, and U. Keller, "240 fs pulses with 22 W average power from a mode-locked thin-disk Yb:KYW laser," Opt. Lett. **27**, 1162–1164 (2002).